



CHORUS

This is the accepted manuscript made available via CHORUS. The article has been published as:

Triplets Contribute to Both an Increase and Loss in Fluorescent Yield in Organic Light Emitting Diodes

Yifan Zhang and Stephen R. Forrest

Phys. Rev. Lett. **108**, 267404 — Published 28 June 2012

DOI: [10.1103/PhysRevLett.108.267404](https://doi.org/10.1103/PhysRevLett.108.267404)

Triplets contribute to both an increase and loss in fluorescent yield in organic light emitting diodes

Yifan Zhang¹ and Stephen R Forrest^{1,2*}

¹Department of Physics, University of Michigan, Ann Arbor, MI 48109

²Department of Electrical Engineering and Computer Science, and Material Science and Engineering, University of Michigan, Ann Arbor, MI 48109

*e-mail: stevefor@umich.edu

Abstract

Non-radiative triplets in fluorescent organic light emitting diodes (OLEDs) can lead to increased efficiency through triplet-triplet annihilation, or to decreased efficiency due to singlet-triplet annihilation. We study the tradeoff between the two processes from the electroluminescence transients of an OLED comprising a tetraphenyldibenzoperiflanthene (DBP) doped rubrene emissive layer, whose emission spectrum peaks at 610 nm. The electroluminescent transients in the current density range, $4 \text{ mA/cm}^2 < J < 57 \text{ A/cm}^2$, are modeled based on singlet and triplet density dynamics. Our analysis shows that triplets positively contribute to the OLED efficiency at $J < 2.2 \text{ A/cm}^2$, while decreasing the efficiency at higher J . The high OLED peak external quantum efficiency of 6.7% and rapid efficiency roll-off with J are quantitatively explained by the tradeoff between triplet-triplet and singlet-triplet annihilation. The model suggests optimal materials properties needed for achieving high efficiency at high brightness in fluorescent OLEDs.

In organic molecular solids, excitons (i.e. bound electron-hole pairs) are responsible for optical transitions. Since an exciton is a two-electron system, it can have a total quantum spin number, S , of zero or one. Depending on the spin degeneracy, an exciton is either a singlet ($S=0$) or a triplet ($S=1$). Since organic molecules typically have a ground state with $S=0$, conservation of spin angular momentum allows only singlets to undergo radiative transitions, with triplets leading to non-radiative processes. In fluorescent organic light emitting diodes (OLEDs), both singlets and triplets are formed when injected carriers recombine, and the formation probability is consistent with the spin degeneracy, i.e. 25% of the recombination forms singlet [1-3]. Thus fluorescent OLEDs were reported to have a theoretical limit to their internal quantum efficiency (*IQE*) of 25% [4]. Recently, two types of excitonic interactions, triplet-triplet annihilation (TTA), and singlet-triplet annihilation (STA) were separately found to significantly influence the efficiency of fluorescent OLEDs. TTA [5, 6] can generate singlets, thus increasing the theoretical limit of the *IQE* from 25%, to a maximum of 62.5% [3, 7-9]. On the other hand, STA [10, 11] reduces the singlet density, thereby lowering the efficiency by as much as 50% at high brightness [12, 13]. However, the relative importance of these two effects has not, to our knowledge, been studied, and the role of triplets remains largely unexplained.

In this work, we study both TTA and STA in a fluorescent OLED based on its electroluminescence (EL) transients. We find that triplets can increase OLED efficiency via TTA at low current density (J), while it decreases the efficiency by STA at high J .

Triplet-triplet annihilation follows one of two pathways [14-16]:



where T is the triplet, S is the singlet, S_0 is the molecular ground state. By conservation of total spin angular momentum, formation of quintets ($\chi=2$) is also an allowed process in TTA; however, since the quintet energy is usually significantly higher than twice the triplet energy, it is typically forbidden at room temperature [15-17]. The rate constants governing the relative importance of processes (1) and (2) are αk_{TT} and $(1-\alpha)k_{TT}$, respectively, where α is the fraction of annihilation events that follow processes (1) vs. (2), k_{TT} is the TTA rate constant. Process (1) contributes to fluorescent OLED efficiency by creating additional singlets from non-radiative triplets. Several recent reports [3, 7, 17] have shown $\alpha > 0$, resulting in fluorescent OLEDs whose *IQE* exceed the 25% spin-statistical limit [1].

Additionally, STA is governed by [14]:



with the rate constant of k_{ST} . Process (1) occurs at rate $\alpha k_{TT}T^2$; process (2) at rate $(1-\alpha)k_{TT}T^2$; and process (3) at rate $k_{ST}ST$. Thus, the singlet and triplet density dynamics are described by:

$$\frac{dS}{dt} = \gamma(J) \frac{J}{4ed} - k_s S - k_{ST}ST + \alpha k_{TT}T^2 \quad (4)$$

$$\frac{dT}{dt} = \gamma(J) \frac{3J}{4ed} - k_T T - (1+\alpha)k_{TT}T^2, \quad (5)$$

where $\gamma(J)$ is the charge balance factor[18, 19], e is the electron charge, d is the charge recombination layer (i.e. emissive layer) thickness, and k_s and k_T are the singlet and triplet natural decay rates. In steady state, the external quantum efficiency, *EQE* can then be calculated from $S(t = \infty, J)$ to give:

$$EQE(J) = \eta_{OUT} \eta_s \frac{k_s S(t = \infty, J)}{J/(ed)}, \quad (6)$$

where η_{OUT} is the out-coupling efficiency [20] and η_s is the radiative efficiency of the singlet.

In rubrene (Fig. 1), the singlet energy ($E_S \sim 2.2$ eV) is twice the triplet energy ($E_T \sim 1.1$ eV), thereby enabling a high, resonant TTA (through process (1)) efficiency [17, 21]. Hence, in our work, tetraphenyldibenzoperiflanthene (DBP) [22, 23] is doped at 1 vol% in rubrene as the OLED emissive layer. During operation, excitons are formed on rubrene through the Coulomb interaction between the injected electrons and holes (a process called charge recombination in organic materials [24, 25]). Then, singlets can resonantly (by Förster process [26]) transfer to DBP and emit. The 1mm^2 square OLEDs were grown on indium-tin-oxide (ITO, as the anode) coated glass substrate by thermal evaporation of organic molecules [27] at a base pressure $< 5 \times 10^{-7}$ Torr. The OLED consists of a 40 nm thick 4,4'-bis[N-(1-naphthyl)-N-phenyl-amino]-biphenyl hole transport layer, a 35 nm thick emissive layer, a 40 nm thick rubrene electron transport layer, a 5 nm thick bathophenanthroline electron injection layer, and a 0.8 nm thick LiF layer followed by a 80 nm thick Al cathode.

The EL transients following current density steps of magnitudes ranging from 4 mA/cm^2 to 57 A/cm^2 , and with rise and fall times of < 20 ns, were measured by an avalanche photodetector and an oscilloscope with < 5 ns time resolution. The current pulse widths were monotonically decreased from $100 \mu\text{s}$ at $J = 4 \text{ mA/cm}^2$ to $5 \mu\text{s}$ at $J = 57 \text{ A/cm}^2$ to ensure the OLED EL intensity reached steady state, but did not undergo thermal or electrical breakdown. The emission intensity at $J = 4 \text{ mA/cm}^2$ was calibrated using a Si photodetector whose area is significantly larger than that of the OLED [28]. All measurements were performed under N_2 ambient.

The OLED shows a peak $EQE = 6.7\%$ at $J = 75 \text{ mA/cm}^2$ (Fig. 2a), clearly exceeding the spin statistically limited $EQE = 5\%$ [4] assuming a random orientation of molecular dipoles.

The EQE undergoes a rapid roll-off with increasing J , decreasing to only 0.9% at 57 A/cm². The EL spectrum of the OLED shows pure DBP emission with a peak wavelength of $\lambda=610$ nm [23], as shown in Fig. 2b, with almost no change over the entire range of J studied.

To understand the high peak EQE followed by a rapid roll-off, we investigated the transient EL response. Figure 3 shows three representative EL transients at 0.023, 11.5 and 49 A/cm². The EL turn-on transients have distinct behaviors at low (Fig. 3a, left) vs. high (Fig. 3c, left) current densities. At low J , the EL intensity gradually increases to a steady state over tens of microseconds. This is consistent with TTA since the triplet density slowly increases over this time scale. In contrast, the transient in Fig. 3c rapidly peaks and then gradually decays to a steady-state intensity approximately 70% of its peak value. This is a signature of STA [12], whereby the singlet density decreases with increasing triplet density. Figure 3b (left) shows a mixture of both TTA and STA. The EL turn-off transients for all current densities show delayed fluorescence (right graphs in Fig. 3) due to TTA [12, 17]. The steady-state EL intensity, EL_{SS} , and the initial delayed fluorescence intensity, EL_{TTA} (see Fig. 3a, right), are related by the ratio, $\rho(J) = EL_{TTA} / EL_{SS}$ (as plotted in Fig. 4), which characterizes the fraction of TTA-generated-emission relative to the total emission intensity.

To quantitatively determine the relative contributions of TTA and STA, Eq's. (4) and (5) are fit to the experimental EL transients (where EL intensity is proportional to S) over 4 mA/cm² < J < 57 A/cm². In these fits, the variables $\gamma(J)$, k_{ST} , and k_{TT} , are unknown, while k_S , k_T , and α can be independently measured. Here, $k_S = 1 / \tau_S = (2.6 \pm 0.1 \text{ ns})^{-1}$ is obtained from the transient photoluminescence data for a 1% DBP: rubrene film [29]. Also, the rate $k_T = 1 / \tau_T = (35 \pm 5 \text{ } \mu\text{s})^{-1}$ is determined from the triplet lifetime, equal to twice the EL decay time constant at

$J=4 \text{ mA/cm}^2$ at $>50 \text{ } \mu\text{s}$ from the current turn-off when TTA is much less efficient than the triplet natural decay [5]. Finally, $\alpha = 0.53$ is obtained from $\rho(J \rightarrow \infty) = 0.51$ (see Fig. 4) using Eq's. (4) and (5):

$$\rho(J) = \frac{3\alpha k_{TT} T^2}{k_T T + (1 + \alpha) k_{TT} T^2 + 3\alpha k_{TT} T^2} \quad (7)$$

where, as $J \rightarrow \infty$, $k_T T$ is negligible, leading to $\lim_{J \rightarrow \infty} \rho = \frac{3\alpha}{4\alpha + 1}$.

According to Giebink, et al. [19], $\gamma(J)$ decreases with increasing J ; hence we assume $\gamma(J) = 1$ at $J=4 \text{ mA/cm}^2$. From these measurements and assumptions, we can accurately determine $\gamma(J)$, k_{ST} , and k_{TT} by fitting the EL transients for all J .

The modeled EL transients closely follow the data in Fig. 3. By including both TTA and STA, the model fits the entire EL transient rather than just the turn-off, as in previous reports [3, 8, 17]. From the fits, we find $k_{ST} = 7.1 \times 10^{-11} \text{ cm}^{-3} \text{ s}^{-1}$, $k_{TT} = 6.0 \times 10^{-14} \text{ cm}^{-3} \text{ s}^{-1}$, and $\gamma(J)$ whose values are shown in Fig. 2a (open circles). According to the density functional calculation of Kondakov, et al. [17], the triplet energy of DBP is $\sim 0.2 \text{ eV}$ higher than the rubrene triplet energy of 1.1 eV ; thus DBP singlets are efficiently quenched by rubrene triplets. Also, since TTA is a short-range Dexter interaction, the high k_{TT} in rubrene suggests a high triplet diffusivity [14]. Finally, we find $\gamma(J) \approx 1$ except at $J > 1 \text{ A/cm}^2$, after which it decreases due to charge leakage through the emissive layer, and field-induced exciton dissociation [19]. The leakage is evident in Fig. 2b, where the emission spectrum shows noticeable increase in the contribution from rubrene (at $\lambda=550\text{nm}$) [30] at $J=62 \text{ A/cm}^2$. We note that exciton-polaron annihilation [12, 14, 31] is also possible in fluorescent OLEDs; however, since inclusion of the process is not needed in the fits to the data, it is not anticipated to play a significant role.

With these experimentally determined rates, steady-state values for S and T are calculated and shown in Fig. 4. The model $EQE(J)$ in Fig. 2a is then derived from S according to Eq. (7) using $\eta_{OUT}\eta_S = 17.3\%$ obtained from the magnitude of $EQE(J)$. The peak $EQE > 5\%$ is a result of TTA, the scale of which can be characterized by ρ , also shown in Fig. 4. At $J < 0.1$ A/cm², $k_{TT}T$ is comparable to k_T and increasing with J , resulting in the monotonic increase of $\rho(J)$. At $J > 1$ A/cm², $k_{TT}T \gg k_T$ and thus ρ saturates according to Eq. (7). In general, the upper limit of IQE is set by, $IQE_{max} = \frac{25\%}{(1-\rho)} = 25\% \times \frac{4\alpha+1}{\alpha+1}$, as plotted in the inset of Fig. 3. For the OLED in this work, $\alpha=0.53$, corresponding to $IQE_{max}=51\%$. When $\alpha=1$, $IQE_{max}=62.5\%$, consistent with the result of Kodakov, et al. [17]. This upper limit can only be reached for $k_{TT}T \ll k_T$ and negligible STA.

To put both TTA and STA into the same context, we define the effective triplet current density as:

$$J_T = \frac{4ed}{\gamma(J)} (\alpha k_{TT}T^2 - k_{ST}ST). \quad (8)$$

Then, Eq. (4) can be simplified to $\frac{dS}{dt} = \gamma(J) \frac{J}{4ed} [1 + \xi] - k_S S$ using the ratio, $\xi = J_T / J$. J_T (and also ξ) can be either positive or negative, depending on whether TTA or STA dominates. Note that when $\gamma(J)=1$, $IQE = 25 \times (1 + \xi)\%$. The calculated ξ for the OLED studied is shown in Fig. 4. With increasing J , ξ is initially positive and increases due to TTA to a peak of $\xi=0.53$ at $J = 50$ mA/cm²; and then decreases due to the increased rate of STA. A critical current density, J_C can be defined when $\xi=0$, and thus the effects of TTA and STA are equal. Above $J_C=2.2$ A/cm², ξ becomes negative and triplets lead to a decrease in quantum efficiency.

The dependence of ξ on J changes with k_{ST} and k_{TT} . In Fig. 5a, ξ vs. J is calculated for different k_{ST} while keeping other parameters constant. As k_{ST} increases, J_c decreases, as does ξ . In contrast, with increasing k_{TT} , both ξ and J_c increase (Fig. 5b). Thus, besides requiring that $E_S \leq 2E_T$ to achieve a large α [17], fluorescent OLEDs with high *EQE* at high brightness also require a large k_{TT} and small k_{ST} . Now k_{TT} is proportional to the triplet diffusivity [14] which increases with crystalline order [32], and k_{ST} is proportional to the overlap between the singlet emission and triplet absorption spectra, [11, 14] providing guidance in choosing materials that can lead to a high efficiency.

Based on J_T , two limiting cases of *EQE* in Fig. 2a are calculated; one for $\alpha=0$ (where TTA does not generate singlets according to Eq. (1)), and the other for $k_{ST}=0$ (no STA). The differences between these calculated *EQE*'s and the data show the relative effects of TTA and STA that are responsible for the high peak *EQE* and rapid roll-off with J , respectively.

Singlet fission is a process in which one singlet shares its energy with a neighboring ground state, and both are converted into triplets [14, 33]. It requires that $E_S \geq 2E_T$. For each absorbed photon, two electron-hole pairs can be harvested, and thus fission has the potential of doubling the efficiency of excitonic solar cells [33-36]. In contrast, TTA through Eq. (1) is the reverse process of singlet fission, where we require that $E_S \leq 2E_T$. For rubrene, the singlet and triplet energies are in resonance, i.e. $E_S=2E_T$ (Fig. 1). In this case, both efficient TTA and singlet fission can co-exist and compete [37]. When a rubrene-only emissive layer is used, then *EQE* < 0.2%, indicating that singlet fission dominates over rubrene emission. On the other hand, resonant (Förster) singlet transfer from rubrene to DBP suppresses rubrene singlet fission, and thus the use of DBP as a dopant yields a peak *EQE* of 6.7%. From another prospective, fast

Förster transfer of singlets represents a significant loss mechanism for singlet fission in excitonic solar cells, and should be avoided in those devices.

In conclusion, we develop a model that accurately describes singlet and triplet density dynamics in fluorescent OLEDs over more than four decades of current density. Based on this model, the dependence of the internal quantum efficiency limits of fluorescent OLEDs on TTA is obtained, explaining the high peak efficiency of 6.7% experimentally observed. The overall effect of triplets, including TTA and STA, is understood by introducing the concept of an effective triplet current density that is used to describe the efficiency roll-off at high current densities and brightness. Our model provides guidance for the appropriate design of molecules and device structures that can be used for high efficiency fluorescent OLEDs as well as organic photovoltaics employing singlet fission.

Acknowledgements

We thank the U.S. Department of Energy, Center for Energy Nanoscience at the University of Southern California (award DE-SC0001013, YZ, experiment, analysis), and a Small Business Innovation Research program subcontract funded by the US Department of Energy through Universal Display Corporation (SRF, analysis, technology transfer) for financial support.

References

- [1] M. A. Baldo *et al.*, Phys. Rev. B **60** 14422 (1999).
- [2] M. Segal *et al.*, Phys. Rev. B **68** 075211 (2003).
- [3] B. H. Wallikewitz *et al.*, Phys. Rev. B **85** 045209 (2012).
- [4] T. Tsutsui, MRS Bull. **22** 39 (1997).
- [5] R. G. Kepler *et al.*, Phys. Rev. Lett. **10** 400 (1963).
- [6] R. P. Groff, R. E. Merrifield, and P. Avakian, Chem. Phys. Lett. **5** 168 (1970).
- [7] D. Yokoyama *et al.*, Appl. Phys. Lett. **99** 123303 (2011).
- [8] S. M. King *et al.*, J. Appl. Phys. **109** 074502 (2011).
- [9] Y. Luo, and H. Aziz, Adv. Funct. Mater. **20** 1285 (2010).
- [10] J. Fourny, G. Delacôte, and M. Schott, Phys. Rev. Lett. **21** 1085 (1968).
- [11] N. C. Giebink, and S. R. Forrest, Phys. Rev. B **79** 073302 (2009).
- [12] Y. Zhang *et al.*, Chem. Phys. Lett. **495** 161 (2010).
- [13] D. Kasemann *et al.*, Phys. Rev. B **84** 115208 (2011).
- [14] M. Pope, and C. E. Swenberg, *Electronic Processes in Organic Crystals and Polymers* (Oxford University Press, New York, 1999), Second edn.
- [15] A. Kohler, and H. Bassler, Materials Science & Engineering R-Reports **66** 71 (2009).
- [16] B. Dick, and B. Nickel, Chem. Phys. **78** 1 (1983).
- [17] D. Y. Kondakov *et al.*, J. Appl. Phys. **106** 124510 (2009).
- [18] B. Ruhstaller *et al.*, J. Appl. Phys. **89** 4575 (2001).
- [19] N. C. Giebink, and S. R. Forrest, Phys. Rev. B **77** 235215 (2008).

- [20] C. Adachi *et al.*, J. Appl. Phys. **90** 5048 (2001).
- [21] M. Montalti *et al.*, *Handbook of Photochemistry* (CRC Press, Boca Raton, FL, 2006), 3rd edn.
- [22] J. D. Debad *et al.*, J. Am. Chem. Soc. **118** 2374 (1996).
- [23] K. Okumoto *et al.*, Appl. Phys. Lett. **89** 013502 (2006).
- [24] R. H. Friend *et al.*, Nature **397** 121 (1999).
- [25] W. Staroske *et al.*, Phys. Rev. Lett. **98** 197402 (2007).
- [26] T. Förster, Radiation Research Supplement **2** 326 (1960).
- [27] S. R. Forrest, Chem. Rev. **97** 1793 (1997).
- [28] S. R. Forrest, D. D. C. Bradley, and M. E. Thompson, Adv. Mater. **15** 1043 (2003).
- [29] R. R. Lunt *et al.*, J. Appl. Phys. **105** 053711 (2009).
- [30] G. Sakamoto *et al.*, Appl. Phys. Lett. **75** 766 (1999).
- [31] M. A. Baldo, R. J. Holmes, and S. R. Forrest, Phys. Rev. B **66** 035321 (2002).
- [32] R. R. Lunt, J. B. Benziger, and S. R. Forrest, Adv. Mater. **22** 1233 (2010).
- [33] M. B. Smith, and J. Michl, Chem. Rev. **110** 6891 (2010).
- [34] P. M. Zimmerman, Z. Zhang, and C. B. Musgrave, Nat Chem **2** 648 (2010).
- [35] J. Lee, P. Jadhav, and M. A. Baldo, Appl. Phys. Lett. **95** 033301 (2009).
- [36] P. J. Jadhav *et al.*, Nano Lett. **11** 1495 (2011).
- [37] A. Ryasnyanskiy, and I. Biaggio, Phys. Rev. B **84** 193203 (2011).

Figure Captions

Figure 1. Energetics of a DBP doped rubrene mixture. In rubrene, the singlet energy, E_S , is twice that of the triplet ($2E_T$). In this case, singlet formation through triplet-triplet annihilation (TTA) is a resonant process. The use of a DBP dopant allows the Förster transfer of singlets from rubrene to DBP, which dominates over rubrene singlet fission.

Figure 2. (a) External quantum efficiency (EQE , squares) and charge balance factor (γ , circles) vs. current density, J for the organic light emitting diode (OLED). The lines correspond to the calculated EQE from the model described in text; i.e. with both TTA and singlet-triplet annihilation (STA) present (solid line), in the absence of TTA (dotted line), and in the absence of STA (dashed line). (b) Emission spectra for the OLED at different J .

Figure 3. Electroluminescence (EL) turn-on (left graphs) and turn-off (right graphs) transients (grey squares) for the DBP doped rubrene OLED under a current density pulse at (a) $J=0.023$ A/cm²; (b) $J=11.5$ A/cm²; and (c) $J=49$ A/cm². The red dashed lines are EL intensities assumed to be proportional to the singlet densities, and black solid lines are the corresponding triplet densities.

Figure 4. Calculated singlet (S) and triplet (T) densities (left axis), experimental (squares) and calculated (solid line) ratios of the delayed fluorescence EL to total EL (ρ , right axis), and the ratio ξ of the effective triplet current density (J_T) to J . Inset: Maximum internal quantum efficiency (IQE_{max}) for fluorescent OLEDs vs. the TTA generation ratio (α). The square shows IQE_{max} for the DBP doped rubrene OLED of this work.

Figure 5. Ratio ξ vs. J , as a function of the (a) STA rate k_{ST} and (b) TTA rate k_{TT} , keeping other parameters as found for the DBP doped rubrene OLED. Here, “0” indicates the contour where triplets show no net contribution to OLED efficiency. Also, ξ changes by 0.15 between adjacent contours.

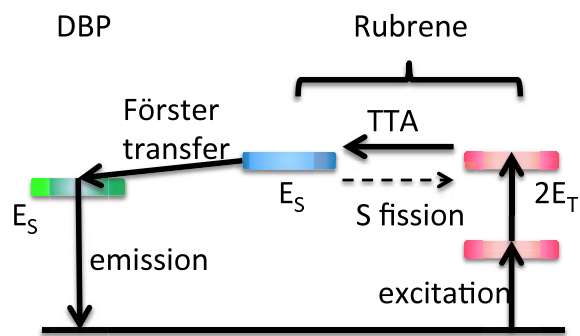


Fig. 1

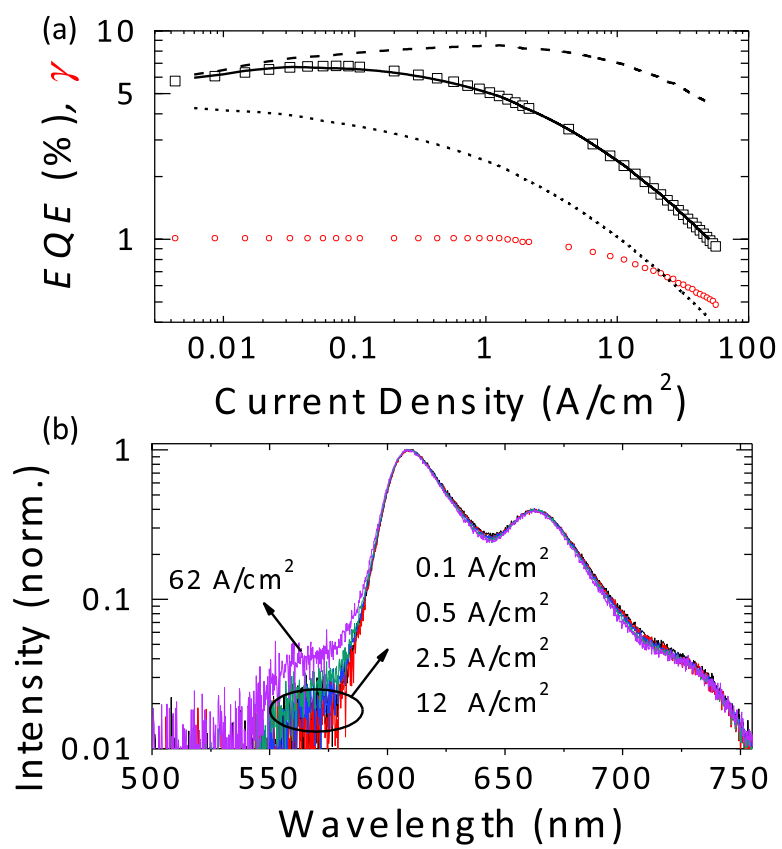


Fig. 2

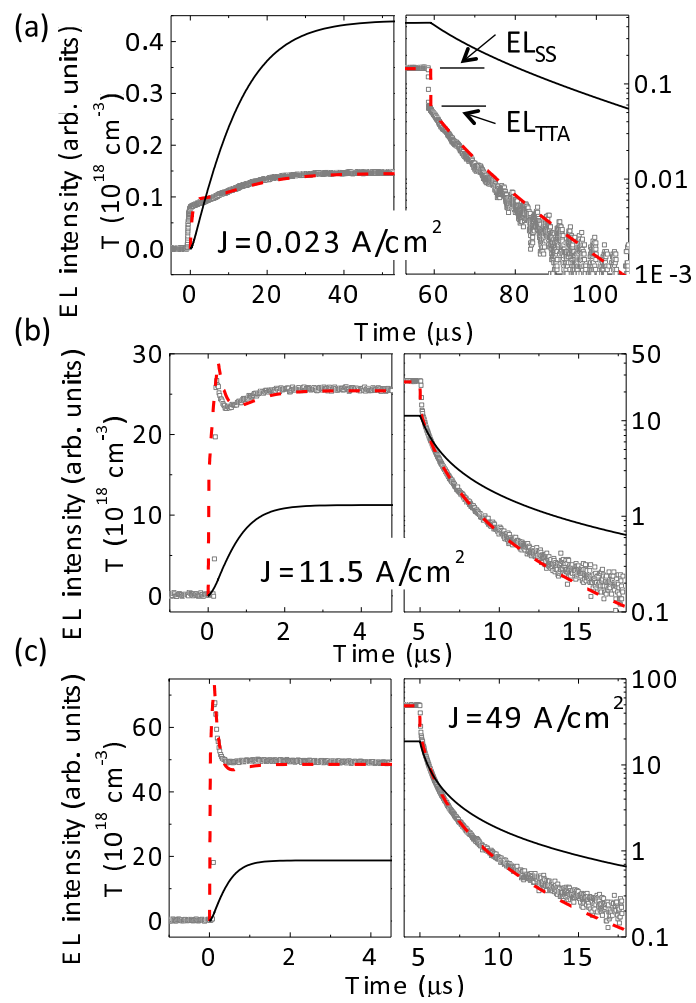


Fig. 3

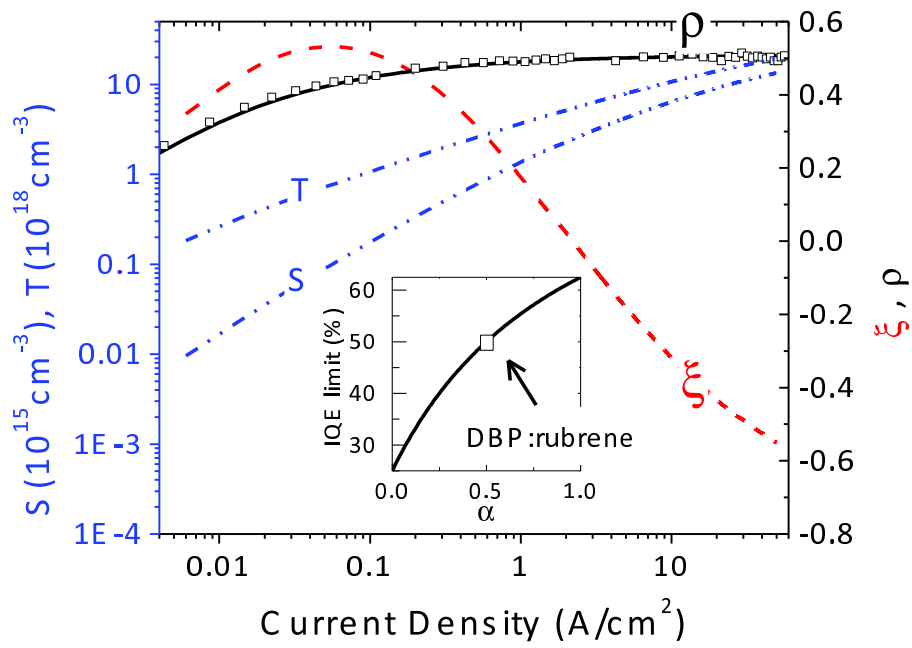


Fig. 4

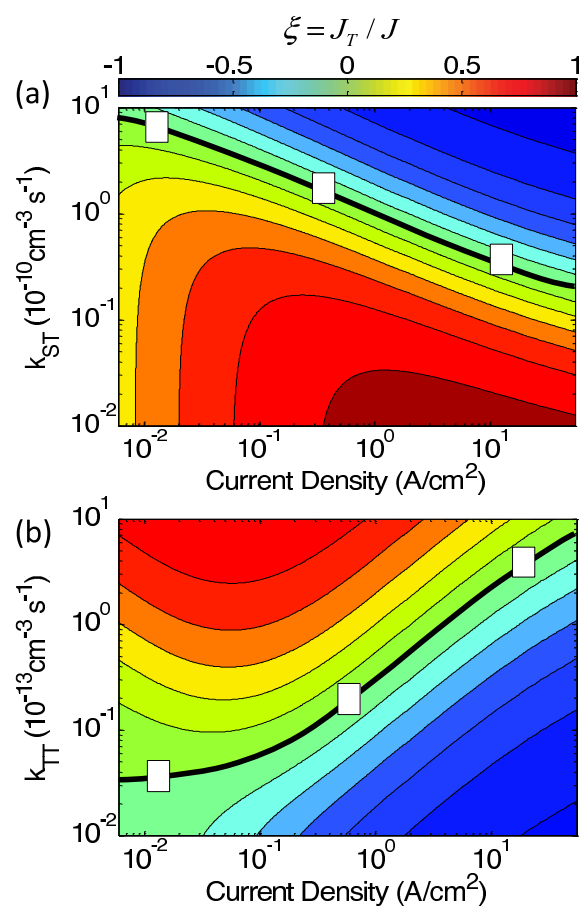


Fig. 5